Remote Sensing of Environment 115 (2011) 1532–1542

Contents lists available at ScienceDirect

Remote Sensing of Environment

journal homepage: www.elsevier.com/locate/rse

An airborne lidar sampling strategy to model forest canopy height from Quickbird imagery and GEOBIA

Gang Chen *, Geoffrey J. Hay

Foothills Facility for Remote Sensing and GIScience, Department of Geography, University of Calgary, Calgary, AB, Canada T2N 1N4

ARTICLE INFO

Article history:
Received 22 February 2010
Received in revised form 8 February 2011
Accepted 13 February 2011
Available online 3 March 2011

Keywords:
Quickbird
Lidar transect
Geographic Object-Based Image Analysis (GEOBIA)
Forest canopy height

ABSTRACT

High-resolution digital canopy models derived from airborne lidar data have the ability to provide detailed information on the vertical structure of forests. However, compared to satellite data of similar spatial resolution and extent, the small footprint airborne lidar data required to produce such models remain expensive. In an effort to reduce these costs, the primary objective of this paper is to develop an airborne lidar sampling strategy to model full-scene forest canopy height from optical imagery, lidar transects and *Geographic Object-Based Image Analysis* (GEOBIA). To achieve this goal, this research focuses on (i) determining appropriate lidar transect features (i.e., location, direction and extent) from an optical scene, (ii) developing a mechanism to model forest canopy height for the full-scene based on a minimum number of lidar transects, and (iii) defining an optimal *mean object size* (MOS) to accurately model the canopy composition and height distribution. Results show that (i) the transect locations derived from our *optimal lidar transect selection algorithm* accurately capture the canopy height variability of the entire study area; (ii) our canopy height estimation models have similar performance in two lidar transect directions (i.e., north–south and west–east); (iii) a small lidar extent (17.6% of total size) can achieve similar canopy height estimation accuracies as those modeled from the full lidar scene; and (iv) different MOS can lead to distinctly different canopy height results. By comparing the best canopy height estimate with the full lidar canopy height data, we obtained average estimation errors of 6.0 m and 6.8 m for conifer and deciduous forests at the individual tree crown/small tree cluster level, and an area weighted combined error of 6.2 m, which is lower than the provincial forest inventory height class interval (i.e., ≈9.0 m).

1. Introduction

Recent studies have proven the feasibility of using lidar (light detection and ranging) data to characterize forest vertical structure (e.g., canopy height), by generating accurate estimates of forest above-ground biomass and timber volume (Hyyppä et al., 2008; Lefsky et al., 2002; Lim et al., 2003; Means et al., 1999). In these cases, promising results were reported using airborne lidar scanners, whose small-footprint and high-pulse-density returns can accurately estimate forest canopy height at the individual tree level. Compared to data acquisition costs from spaceborne sensors, the cost associated with airborne lidar data is highly influenced by several critical — but varying — factors, such as the project location, topography, the number of flight turns and banks, distance between lidar transects and pulse density, etc.

To reduce airborne acquisition costs while still collecting useful estimates of forest vertical structure, research is beginning to be conducted on the integration of airborne lidar transects and high-resolution optical remotely sensed data. For example, Hudak et al. (2002) combined lidar data and Landsat ETM+ panchromatic imagery to estimate forest canopy height in western Oregon, USA. Here, a lidar canopy height model was sampled in both transect and point patterns with equal spatial intervals of 2000, 1000, 500, and 250 m. Best results were reported by using lidar samples with smaller spatial intervals. Similarly, Wulder and Seemann (2003) developed regression models between lidar and Landsat TM data to estimate canopy height at the stand level. This relationship was then extended to polygons without lidar data to predict/update canopy height inventory information. Their models revealed a correlation (R^2) of 0.61 between digital numbers (DNs) and associated lidar-estimated heights for segmentation-derived polygons. Hilker et al. (2008) further investigated the potential of combining small-footprint lidar transect data and QuickBird imagery to update forest inventories. They found a strong relationship ($R = 0.89$) between the stand height predicted from a single lidar transect and Quickbird imagery, and the stand height from the full-area lidar coverage. Though encouraging results have been obtained by integrating lidar transects and optical imagery, several important lidar transect features such as location, direction and extent are still heuristically defined, which ultimately could decrease the accuracy of estimating canopy height for the whole

* Corresponding author. Tel.: +1 4032108761.
E-mail address: gangchen@ucalgary.ca (G. Chen).

0034-4257/$ – see front matter © 2011 Elsevier Inc. All rights reserved.
doi:10.1016/j.rse.2011.02.012

study area. This is because heuristically defined lidar transect locations may fail to represent the height structure of the full-scene — especially over large areas. Therefore, decisions regarding the appropriate selection of lidar transect features are critical for developing robust integrated models.

At a high spatial resolution (<5.0 m), individual pixels typically represent only a small portion of the geographic objects of interest (e.g., individual trees). While this resolution provides details that can further facilitate landscape management, it also creates higher internal spectral variance within each geographic object which can decrease scene model accuracy when using pixel-based approaches (Hay et al., 1996; Strahler et al., 1986). To acquire detailed geographic information while minimizing the effect of high internal spectral variance, *Geographic Object-Based Image Analysis* (GEOBIA) provides a feasible alternative to the traditional pixel-based approach (Hay & Castilla, 2008). GEOBIA is essentially a way to move from the analysis of individual pixels to image-objects (i.e., groups of connected pixels that are relatively homogeneous and different from their surroundings), to the generation of geo-intelligence (i.e., spatial content within context) (Hay & Blaschke, 2010). In high-resolution remote sensing studies, image-objects can be used to represent forest entities ranging from small tree clusters to large stands, etc. Compared to the traditional pixel-based approach, segmented objects are more similar to forest inventory polygons and easier to use within a GIS, and/or modeling environment.

Based on these ideas, the main objective of this research is to develop an airborne lidar sampling strategy to model full-scene forest canopy height from optical imagery, lidar transects and GEOBIA. To achieve this goal, the following sections provide detail regarding (i) data processing; (ii) how GEOBIA was used to define an optimal *mean object size* (MOS) for modeling canopy pseudo-height distribution; (iii) a description of the methods developed to define appropriate lidar transect features (i.e., location, direction and extent) from an optical scene; and (iv) how we modeled full-scene forest canopy height based on a minimum number of lidar transects. Results are then provided and discussed, followed by our conclusions and future work.

2. Data and preprocessing

2.1. Study area

Our study site is located (49°52′N, 125°20′W) approximately 10 km southwest of Campbell River on Vancouver Island, British Columbia, Canada (Fig. 1). The size of the study area is 5.1×5.1 km (2601 ha) and is characterized by conifer and deciduous forests, clearcuts, roads and a river. The study area is comprised of 65% conifer forests, of which ≈80% is dominated by Douglas-fir [*Pseudotsuga menziesii* (Mirb.) Franco], along with small proportions of Western Red Cedar [*Thuja plicata* (Donn.)] and Western Hemlock [*Tsuga*

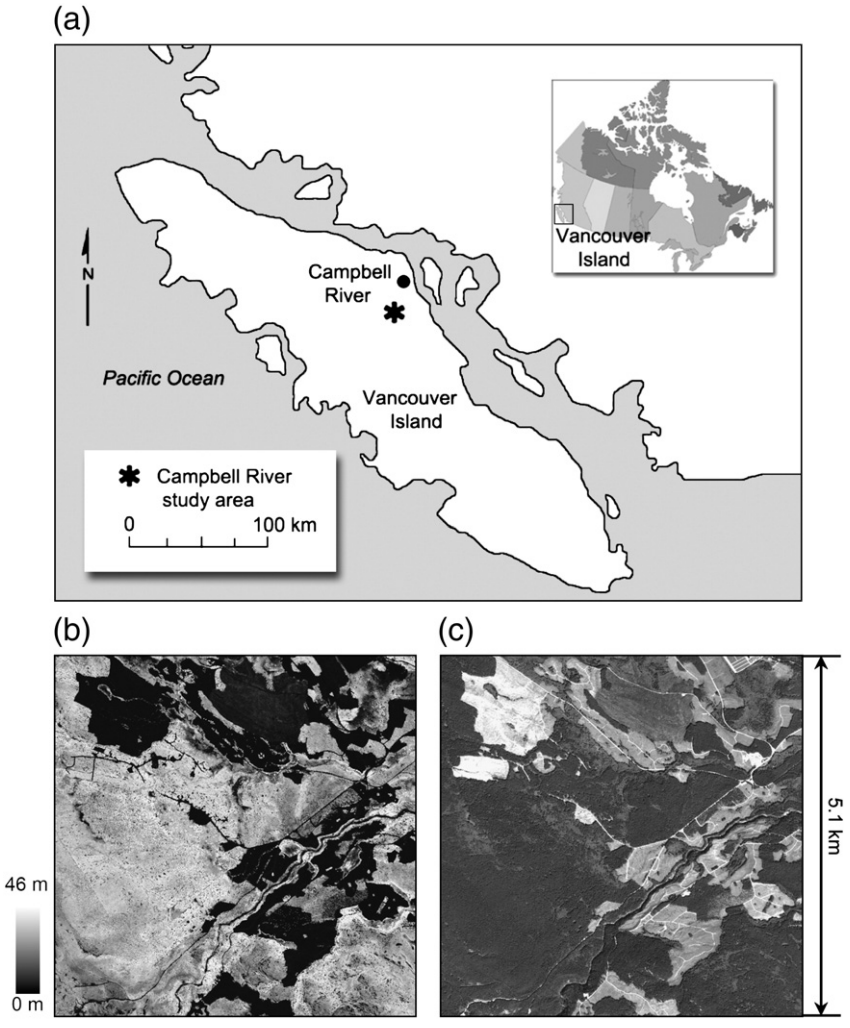

Fig. 1. (a) Study area located southwest of Campbell River, Vancouver Island, Canada. (b) Lidar canopy height segmentation image (CHS). (c) Quickbird grayscale image converted from a false color composite using near infrared (NIR), red and green bands.

heterophylla (Raf.) Sarg.] (Morgenstern et al., 2004). Another 16% of the study area is dominated by Red Alder (*Alnus rubra* Bong.), with the rest of site composed of clearcuts, roads and a river that diagonally bisects the site from southeast to northwest (Morgenstern et al., 2004). Topographically, the site has an average elevation of 300 m above sea level, ranging from 180 m (southwest) to 440 m (northeast), with a gentle slope of 5°–10° except at the river where elevation varies (+/−25 m).

2.2. Lidar data

Lidar data were acquired on June 8, 2004, by an airborne Terrain Scanning Lidar system (Terra Remote Sensing Inc., Sidney, Canada). As a discrete return lidar system (Lightwave Model 110), this system has a pulse repetition frequency of 10 kHz, a wavelength of 1047 nm, a swath width of 56°, and a beam divergence of 3.5 mrad. A continuous scanning mode in the typical zigzag pattern was used during data acquisition, with a footprint size of 0.19 m and a point density of 0.7/m^2 (Hilker et al., 2008). A lidar *digital elevation model* (DEM) and a *digital surface model* (DSM) were generated at a 1.0 m spatial resolution and delivered by the data vendor. A forest canopy height model (CHM) was then derived by subtracting the DEM from the DSM.

2.2.1. Canopy height segmentation (CHS)

While a lidar CHM characterizes forest height at the per-pixel level, such a model fails to represent actual forest entities (i.e., individual trees). To overcome this limitation, a watershed segmentation was applied to the CHM to create a *canopy height segmentation image* (CHS), which visually contained segmented objects that well represented *individual tree crowns* or *small tree clusters*. Watershed segmentation was conducted by (i) searching tree tops in the CHM based on a local maximum algorithm, (ii) flooding (inverted) canopy areas using a watershed algorithm (Dougherty & Lotufo, 2003), (iii) indentifying canopy crowns using a 2.0 m height threshold, and (iv) filling each crown/canopy area with the corresponding average CHM pixel values. *Average height* was used based on previous studies that show a strong relationship between the average height of lidar returns and above-ground forest biomass and volume (Lefsky et al., 2002; Lim et al., 2003). Table 1 illustrates the proportion of each forest canopy height class in the study area; where the height classes were adopted from the British Columbia forest inventory height class codes (MFR, 2010). To remove non-tree components such as low bushes and shrubs, our height range started from 2.0 m instead of 0.0 m.

2.3. Quickbird (QB) data

A cloud-free QB image of the study site was acquired on August 11, 2004. Four multispectral bands [i.e., blue, green, red and near infrared (NIR)] and one panchromatic band were used in this study.

A principal components spectral sharpening technique (Welch & Ahlers, 1987) was used to combine and resample (to 1.0 m) the spectral information from the QB multispectral bands and the spatial information from the QB panchromatic band, as this method maintains the integrity of the original DNs. The lidar and pan-sharpened optical data were then geometrically co-registered using the CHS as the base. A second-order polynomial warping method and nearest neighbour resampling were applied based on 118 tie points, yielding a RMSE of 0.85 m. Due to the dense forest cover in this area, co-registration was performed using tree tops only.

Table 1
Forest proportion of each lidar-measured canopy height class in the study area.

Canopy height class (m)	Forest proportion (%)
2–10.4	7.41
10.5–19.4	25.11
19.5–28.4	56.47
28.5–37.4	10.94
37.5–46.4	0.07

3. Data analysis

An important consideration of this research was to exploit the canopy height variability inherent within the high-resolution optical scene, and use it as a guide for selecting the most appropriate locations to extract lidar transects. Though seldom explored in the remote sensing literature (Hay, 1993), visual depth and height information are readily available from a monocular image via: size perspective (diminution of size with distance), motion parallax, areal perspective (haziness associated with distance), occlusion effects, outline continuity (complete objects look closer), and surface shading variations (Horn & Brooks, 1989; Jarvis, 1983). Furthermore, high-resolution optical data have shown promise in previous forest studies to estimate tree height (Donoghue & Watt, 2006; Franklin & McDermid, 1993; Hyde et al., 2006).

To exploit this inherent optical-height relationship, a multiscale segmentation was first applied to the QB imagery. Using 'structural' information exclusively derived from this QB segmentation, we then created a *pseudo canopy height map*, from which optimal lidar transect locations were selected. We also compared the performance of different models that employed various lidar transect extents with the full-scene lidar dataset. Different sizes of canopy objects (derived from GEOBIA) and their sensitivity to height estimation accuracies were further analyzed. The flowchart in Fig. 2 summarizes these steps; while the following sub-sections provide greater detail and explanation.

3.1. Multiscale segmentation

The basic areal units for GEOBIA are segmentation-derived partitions (a.k.a., *geo-objects*), which represent delineated areas, entities or objects in the image that are meaningful to the analyst and have a geographic referent. In this study, automated image segmentation software — *Size-Constrained Region Merging* (SCRM) (Castilla et al., 2008) was applied to the pan-sharpened multispectral QB data. Compared to currently existing segmentation algorithms, key advantages of SCRM are: (i) the size (e.g., mean, minimum and maximum area) of the objects of interest can easily and explicitly be controlled through input parameters; and (ii) smooth pixel boundaries can be generated, which results in objects (i.e., polygons) similar to those delineated by experienced forest analysts. SCRM contains six main processing steps: image resampling, image smoothing, gradient magnitude image generation, watershed partitioning, region merging and vectorization (Hay et al., 2005).

A forest is a complex system composed of different sized, shaped and spatially distributed entities of interest that is seldom fully characterized at a single scale of analysis. To investigate the optimal *mean object size* (MOS) to estimate canopy height, SCRM was applied to the pan-sharpened QB data to generate 15 derived (multiscale) images composed of different sized canopy-objects, ranging from 0.04 ha to 6.00 ha. Table 2 list the SCRM parameters used, which were chosen to avoid under- and over-segmentation of visibly distinct canopy components within the QB imagery. They also follow a scale range that often appears in natural systems (Hay et al., 2001; O'Neill et al., 1996).

3.2. Canopy-object pseudo-height classification

An important objective of this research was to determine appropriate locations to acquire lidar transects. Therefore, lidar data cannot be used at this stage of analysis. However, it is necessary to have a general idea of how canopy height is distributed in the study

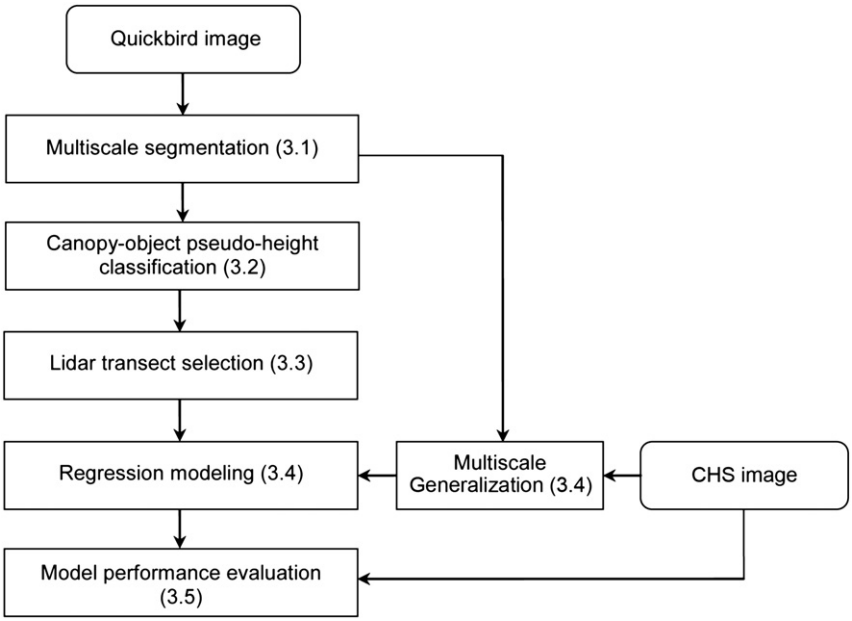

Fig. 2. Flowchart of the research process with reference to Data analysis section.

area. Otherwise, lidar data sampling will be arbitrary, with the possibility of completely omitting the height class(es) of interest. In this step, QB imagery was used to simulate the canopy composition and height variability for the entire study area. This was based on previous research (Chen et al., 2010), which demonstrated the utility of applying high-resolution QB data to estimate lidar-measured forest canopy height from three types of QB-derived object-based variables: (i) *spectral mean* (i.e., mean of the DNs within segments for each spectral band — blue, red, green and NIR); (ii) *image-texture* of the spectral bands, which includes (a) *internal-object texture* — a measure of the spatial variability of DNs within a segmented object, and (b) *geographic object-based texture* (GEOTEX) — a measure of the spatial variability within neighbouring objects (see Fig. 3); and (iii) *shadow fraction* — a quotient of the size of shaded areas and the size of the corresponding forest objects based on the DNs of the NIR band. These variables were calculated from the QB data following the methods of Chen et al. (2010).

An ISODATA unsupervised classification algorithm (Tou & Gonzalez, 1974) was then applied to these variables to generate 14 pseudo-height classes using an iteration number of 20. The choice of class number was based on seven corresponding British Columbia forest inventory height classes (MFR, 2010) for two forest types (conifer and deciduous).

We note that QB data, segmented at the smallest MOS of 0.04 ha, were used in this canopy-object pseudo-height classification step. This was because the *within-object* canopy height variability was found to be relatively low with this MOS (Fig. 4), resulting in a high *between-object* variability. This ensured that canopy height and composition variability [i.e., deciduous (35%) versus coniferous (65%)] were well modeled by the (0.04 ha) segmented image, which was necessary for accurate lidar transect selection.

3.3. Lidar transect selection

Lidar transect selection was defined by employing the canopy pseudo-height classification result as a proxy for forest height class variability. Based on our actual lidar data acquisition parameters, a lidar swath width of 450 m (representing 8.8% of the total study area) was used as the minimum transect size. Three main rules were applied to select candidate lidar transects: (i) transects must contain no overlap with other transects; (ii) transect-covered areas must sample all canopy-object pseudo-height classes (with the non-vegetated objects masked out prior to analysis); and (iii) the canopy

Table 2
Segmentation parameters used in SCRM.

Scale	Minimum object size (ha)	Mean object size (ha)	Maximum object size (ha)
1	0.008	0.040	0.048
2	0.030	0.150	0.180
3	0.070	0.350	0.420
4	0.130	0.650	0.780
5	0.200	1.000	1.200
6	0.300	1.500	1.800
7	0.400	2.000	2.400
8	0.500	2.500	3.000
9	0.600	3.000	3.600
10	0.700	3.500	4.200
11	0.800	4.000	4.800
12	0.900	4.500	5.400
13	1.000	5.000	6.000
14	1.100	5.500	6.600
15	1.200	6.000	7.200

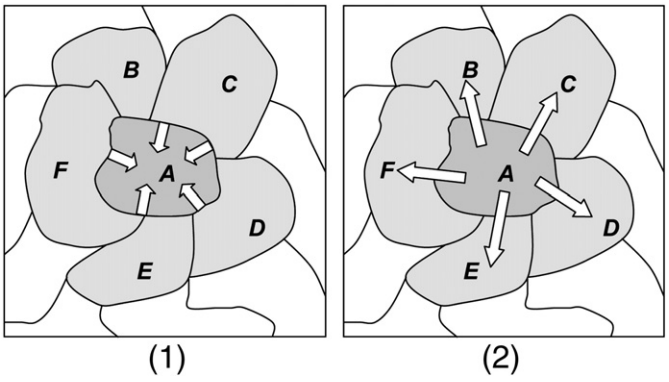

Fig. 3. Two types of texture measures: (1) an internal variability measure calculating standard deviation of DNs within an object (A), and (2) a geographic object-based texture (GEOTEX) measure for object (A) based on calculating the standard deviation of DNs averaged within neighbouring objects — A, B, C, D, E and F.

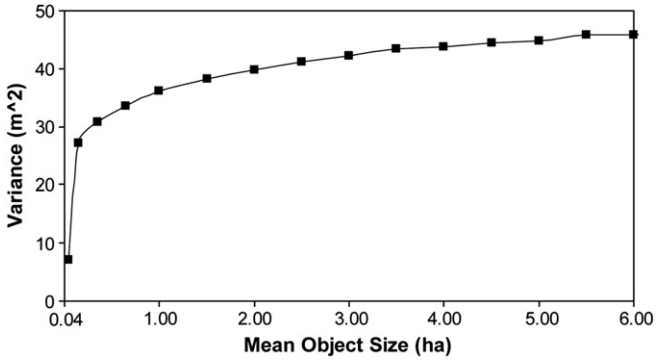

Fig. 4. Canopy height *within-object* variance derived from lidar CHM for all 15 MOS.

pseudo-height histogram derived from the transect-covered objects must have the highest correlation with the pseudo-height histogram derived from all objects.

Transect selection involved comparing 11 different sizes (and locations) of transect extents, each defined as a percentage of the total study area: (1) 8.8%, (2) 17.6%, (3) 26.4%, (4) 35.2%, (5) 44.0%, (6) 52.8%, (7) 61.6%, (8) 70.4%, (9) 79.2%, (10) 87.4% and (11) 100.0% — the full lidar scene. The transect locations were determined by meeting the previously defined lidar transect selection rules within an iterative process. Lidar transect selection performance was evaluated based on two orthogonal directions: N–S (north–south) and W–E (west–east).

3.4. Regression modeling

Building upon previous research (Chen et al., 2010), nonlinear stepwise regression models (formulated using a combination of exponential and quadratic form) were used to develop multiscale relationships (i.e., using 15 MOS) between QB and lidar forest-objects within the lidar transect areas:

$$CH = exp\left(\sum_{i=0}^{n}\left(a_i X_i^2 + b_i X_i + c_i\right)\right) + \varepsilon_i \quad (1)$$

where *CH* is the *canopy height* — extracted from the canopy height segmentation image (CHS — Section 2.2.1); X_i is the *i*th independent variable (derived from the QB scene), which includes the same three QB variables used in Section 3.2; a_i, b_i and c_i are coefficients for the *i*th variable; *n* is the number of independent variables; and an error term, ε_i.

To evaluate canopy height information at multiple scales, the CHS was generalized using 15 different mean object sizes (MOS) (Table 2). Specifically, object boundaries derived from the 15 previously segmented QB images (Section 3.1) were overlaid onto the CHS; then each object was filled with the average CHS values within its extent. The CHS image was used rather than the original CHM because we wanted to understand the effect of canopy objects, not arbitrarily located individual pixels. Additionally, canopy objects reduce the bias caused by non-canopy pixels (i.e., gaps and barren ground, etc.).

Different forest types (e.g., deciduous and conifer) reveal different spectral reflectance characteristics within the QB imagery. In

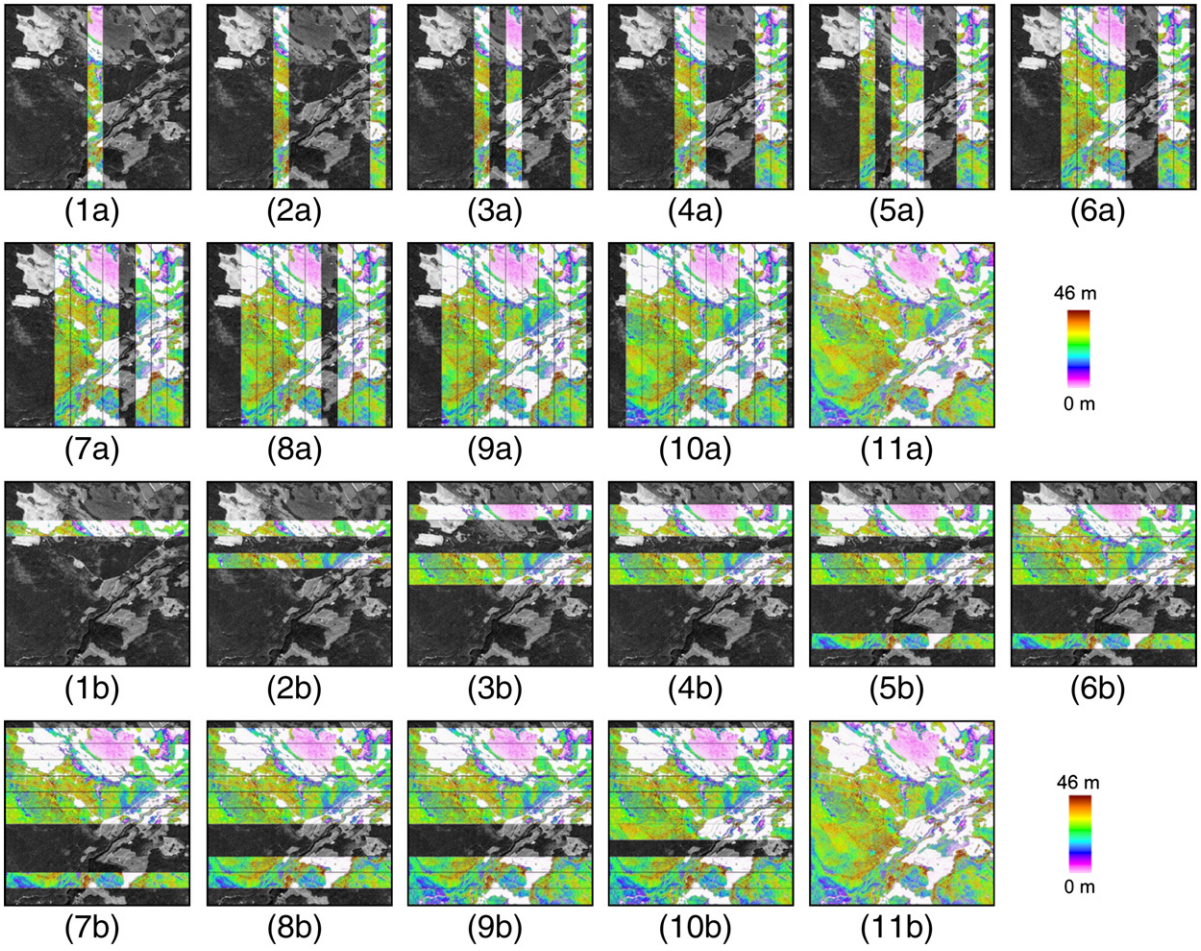

Fig. 5. Examples of 22 combinations of lidar transects derived from the lidar transect selection algorithm (Section 3.3), which represent various transect numbers and their (%) extent: (1) 8.8%, (2) 17.6%, (3) 26.4%, (4) 35.2%, (5) 44.0%, (6) 52.8%, (7) 61.6%, (8) 70.4%, (9) 79.2%, (10) 87.4% and (11) 100.0%. Directions of N–S and W–E are designated with the subscripts (a) and (b) respectively. For illustrative purposes, the QB image was used as the base layer with lidar transects overlaid.

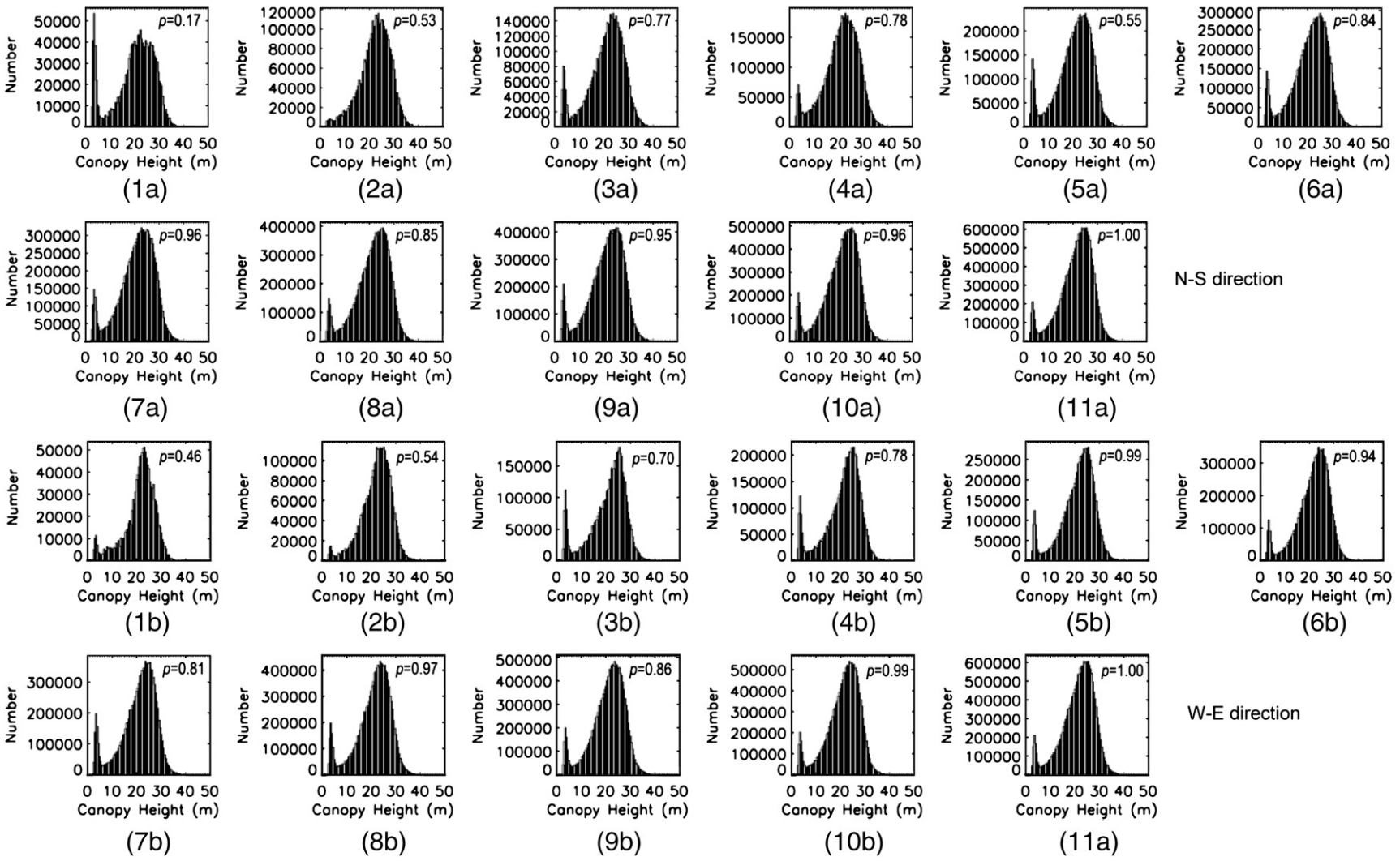

Fig. 6. Canopy height histograms derived from the selected lidar transects (in Fig. 6) for 22 combinations representing various transect numbers and their (%) extent: (1) 8.8%, (2) 17.6%, (3) 26.4%, (4) 35.2%, (5) 44.0%, (6) 52.8%, (7) 61.6%, (8) 70.4%, (9) 79.2%, (10) 87.4% and (11) 100.0%, in (a) N–S and (b) W–E directions.

particular, conifers typically have lower NDVI (Normalized Difference Vegetation Index) values than deciduous trees. There are two main reasons for this: first, the leaf cell structure of conifers produces smaller reflectance differences between red and NIR bands (Lillesand et al., 2007). Second, conifer stands contain more gaps and crown shadows than deciduous forests. Therefore, two NDVI thresholds (i.e., 0.55 and 0.70) were heuristically defined to classify our study area into three classes: conifers, deciduous, and non-vegetated. Then separate regression models were developed for conifer and deciduous canopies. To assess the NDVI threshold accuracy, 90 points were randomly extracted from each class and manually interpreted as the reference data. An overall accuracy of 86.7% was achieved, with an overall kappa statistic of 0.8.

To better understand the relationship between the lidar transect features (i.e., location, direction and extent) and the canopy height estimation using various MOS, we tested three cases: using (i) 11 different transect extents (Section 3.3); (ii) two transect directions (N–S and W–E), and (iii) 15 different MOS (Section 3.1). In total, 330 models (i.e., $11\times2\times15$) were generated and tested for each forest canopy type. Processing was completed in 2 h using a quad core 2.33 GHz workstation and 16.0 GB RAM.

3.5. Model performance evaluation

The model performance of canopy height estimation for the entire study area was determined by comparing the model-derived canopy height with the canopy height segmentation (CHS) data of the full scene using an object area-weighted RMSE (Chen et al., 2010):

$$RMSE_{Area-weighted} = \sqrt{\frac{1}{A_N}\sum_{i=1}^{N} A_i\left(CH_{QB\_i}-CH_{Lidar\_i}\right)^2} \quad (2)$$

where $RMSE_{Area\text{-}weighted}$ is the area-weighted RMSE; CH_{QB_i} is the canopy height calculated from the regression model using QB imagery for the ith object; CH_{Lidar_i} is the canopy height measured from the lidar CHS for the ith object; A_i is the area size for the ith object; A_N is the forest-covered area, and N is the number of objects.

Since the CHS was generated at the small tree/cluster level, model performance was also evaluated at this level. To facilitate the extension of canopy height information from the area covered by lidar transects to areas without transects, we needed to understand whether the best MOS (i.e., corresponding to the lowest model error) derived from the optimal lidar transect(s) was still the best for the entire study area. Therefore, we examined the sensitivity of model performance on MOS by comparing canopy height estimation accuracy for two cases: (i) models that were applied to the entire study area; and (ii) models that were applied only to lidar transect-covered areas.

4. Results and discussion

4.1. Lidar transect features (location, direction and extent)

In our study area, canopy height estimation accuracy was affected by three lidar transect features: (i) location, (ii) direction and (iii) extent. More detail on these features is provided in the following sub-sections.

4.1.1. Transect location

Fig. 5 illustrates 22 transect combinations in N–S and W–E directions. The QB image is displayed as the base layer, with lidar transects overlaid. Canopy heights within transect locations are displayed using different colors representing height variability. It should be noted that each combination image illustrates the best transect locations (per % study area) derived from our lidar transect selection algorithm (Section 3.3). We note that the lower left portion of the study area is occupied by relatively homogenous forests, which exhibit low canopy height variability. However, other areas (e.g., forest stands close to clearcuts) contain much higher canopy height variability. Fig. 5 visually confirms that the selected lidar transects consider this condition by sampling areas with greater height variability.

Ideally, the 'best' lidar transect location(s) will represent canopy height variability similar to that derived from the entire lidar dataset. To test this condition, Fig. 6 shows the canopy height histograms derived from the same 22 lidar transects (in N–S and W–E directions) illustrated in Fig. 5. The Chi-square test was performed to compare the transect-covered canopy height distributions with those derived from the *full* lidar coverage (see histograms 11a and 11b in Fig. 6). All histograms were discretized to five height classes (Table 1), with values normalized to the range of 1 to 100. The calculated one-tailed probability values (p values) are all higher than 0.05 (Fig. 6), which states that there is no significant difference between the two types of height distributions using the transect selection algorithm and the full lidar coverage. Thus, the transect locations determined by our algorithm well model the visual and statistical canopy height variability of the entire study area.

4.1.2. Transect direction

In this site, the canopy height estimation models have similar performance in N–S and W–E directions. This implies that the spatial distribution of forest canopy height in our study area is similar in

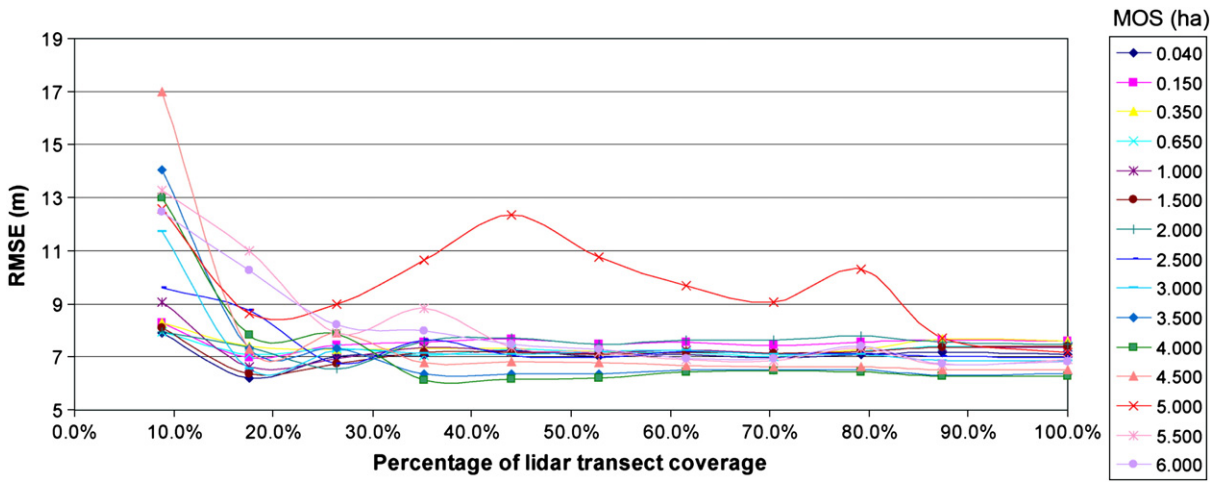

Fig. 7. Canopy height estimation errors derived from 11 combinations of lidar transects with 15 MOS (N–S direction only).

these two directions. Typically, forests are complex ecosystems, which are unlikely to exhibit (N–S or W–E) direction-specific canopy height distribution patterns over a large area. To simplify the remaining discussion, only those results derived from the N–S direction will be presented in the following sections.

4.1.3. Transect extent

The performance of the canopy height estimation models for the entire study area is summarized in Fig. 7. This graph compares the model accuracies of 11 different transect combinations using 15 MOS in the N–S direction. When a small number of lidar transects are chosen, canopy height estimation errors (represented by the RMSE) derived from small object sizes tend to be much lower than those derived from large object sizes. For example, the RMSE is 7.9 m with a MOS of 0.04 ha; however, it is 12.5 m at the MOS of 6.0 ha. By using more transects, canopy height estimation errors decrease at most MOS. However, it should be noted, there exist two transect extent thresholds of 17.6% and 35.2%, where several MOS represent low estimation errors. For example, the RMSE is 6.20 m with a MOS of 0.04 ha and a 17.6% extent; while it is 6.10 m with a MOS of 4.00 ha and a 35.2% extent. Beyond 35.2%, increasing transect cover appears unlikely to affect the model performance of any MOS. Since a smaller transect area represents reduced lidar acquisition and processing costs, the transect size of 17.6% (RMSE: 6.20 m) is selected as optimal for this study.

The above observations can be further explained by the correlation of canopy height variability between transect-covered and full-scene lidar data. Fig. 8 illustrates the correlation derived from 11 transect combinations using 15 MOS in the N–S direction. Typically, a small transect extent (e.g., 8.8%) tends to decrease model performance, because it is unlikely to fully cover canopy height variability within a complex scene. This is especially true, when larger MOS are used within smaller transects, as the number of different object samples (i.e., object variability) within the transect(s) tends to be less, resulting in poorer canopy estimation performance than those using a smaller MOS.

4.2. Evaluation of MOS and models

In order to further evaluate the change of model performance at various MOS, Fig. 9 provides a comparison of the canopy height estimation errors when models were applied to three transect extents (17.6%, 35.2% and 70.4%). We note that the two trend lines in Fig. 9(a)

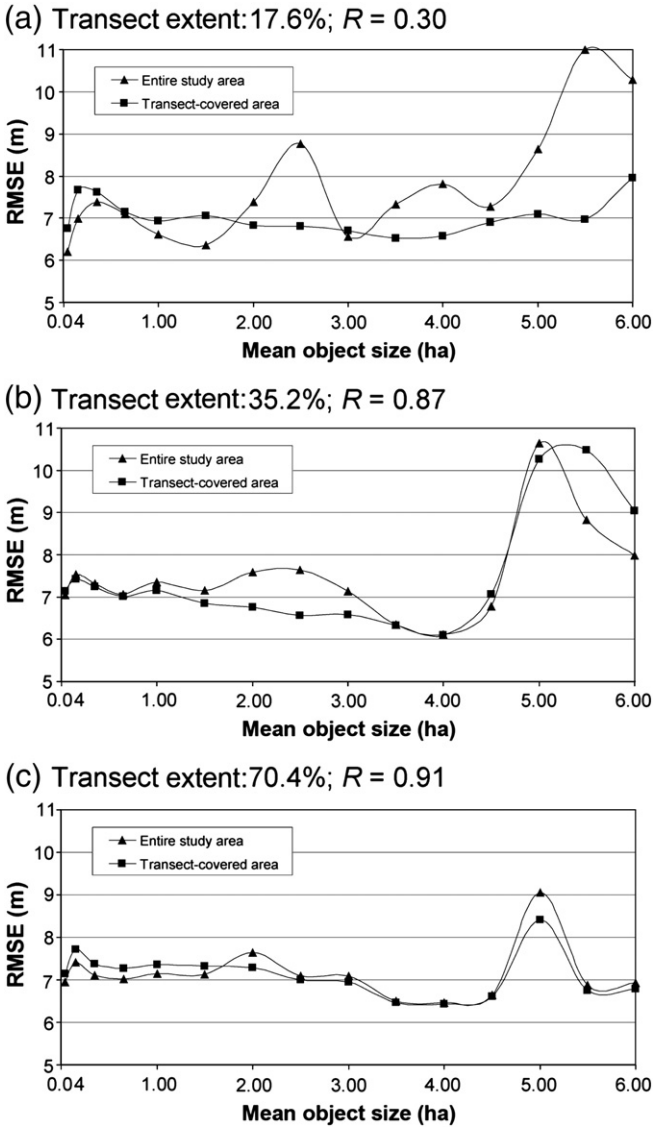

Fig. 9. Comparison of canopy height estimation accuracy when models are applied to the entire study area versus the transect-covered area using examples of (a) 17.6%, (b) 35.2%, and (c) 70.4% transect extents (N–S direction only).

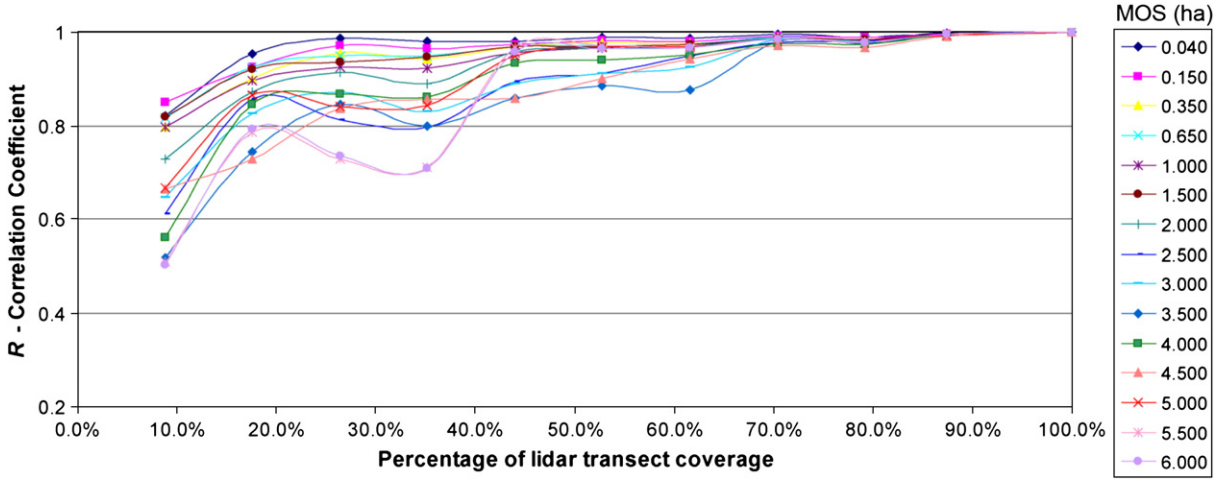

Fig. 8. Correlation between transects and full-scene lidar canopy heights derived from 15 MOS using 11 different combinations of lidar transects (N–S direction only).

Table 3
Regression models for estimating canopy height of (a) conifer and (b) deciduous trees derived from a lidar transect extent of 17.6% and a MOS of 0.04 ha.

Coefficient	Value	Standard error	P value
(a) $Con\_CH = \exp\ (a_0 + a_1 \cdot DN2 + a_2 \cdot TXIT3 + a_3 \cdot TXIT4 + a_4 \cdot GEOTEX1 + a_5 \cdot SF + a_6 \cdot DN2^2 + a_7 \cdot TXIT3^2 + a_8 \cdot TXIT4^2 + a_9 \cdot GEOTEX1^2 + a_{10} \cdot SF^2)$			
a_0	−0.86721	0.46168	<0.05
a_1	0.05227	0.00501	<0.001
a_2	−0.04972	0.00771	<0.001
a_3	0.00505	0.00133	<0.001
a_4	−0.03926	0.00285	<0.001
a_5	2.64657	0.15483	<0.001
a_6	−0.00019	0.00001	<0.001
a_7	0.00160	0.00019	<0.001
a_8	−0.00003	0.00001	<0.001
a_9	0.00098	0.00008	<0.001
a_{10}	−2.29009	0.12849	<0.001
(b) $Dec\_CH = \exp\ (b_0 + b_1 \cdot DN2 + b_2 \cdot TXIT4 + b_3 \cdot GEOTEX1 + b_4 \cdot GEOTEX4 + b_5 \cdot SF + b_6 \cdot DN2^2 + b_7 \cdot TXIT4^2 + b_8 \cdot GEOTEX1^2 + b_9 \cdot GEOTEX4^2 + b_{10} \cdot SF^2)$			
b_0	0.09573	0.00225	<0.001
b_1	0.01312	0.00391	<0.001
b_2	0.01777	0.00318	<0.001
b_3	−0.09401	0.01321	<0.001
b_4	0.02462	0.00220	<0.001
b_5	1.98815	0.93306	<0.05
b_6	−0.00005	0.00001	<0.001
b_7	−0.00008	0.00001	<0.001
b_8	0.00246	0.00055	<0.001
b_9	−0.00012	0.00001	<0.001
b_{10}	−2.42943	1.10310	<0.05

Con_CH = canopy height for conifers; *Dec_CH* = canopy height for deciduous trees; *DN2* = green band; *TXIT3* = red band internal-object texture measure; *TXIT4* = NIR band internal-object texture measure; *GEOTEX1* = blue band GEOTEX; *GEOTEX4* = NIR band GEOTEX; SF = shadow fraction.

have a weak relationship (i.e., $R = 0.30$); however, with the increase of transect extent, the relationship tends to be stronger (Fig. 9(b) and (c)).

As noted in Section 4.1.3, two lidar extent thresholds of 17.6% and 35.2% (and a MOS of 0.04 ha) lead to canopy height estimation errors of 6.20 m and 6.10 m respectively, for the entire study area. Though the smaller lidar extent of 17.6% (Fig. 9(a)) can dramatically reduce lidar data acquisition and processing costs, determining the best MOS is difficult when the correlation is so low (R = 0.30). For example, In Fig. 9(a), the MOS of 2.5 ha produces a RMSE of 6.8 m for the transect-covered area; while a larger RMSE of 8.8 m is introduced by using the same MOS for the entire study site. Consequently, there exists a risk when arbitrarily selecting a small lidar transect, as the canopy height estimation errors may be different for the sampled area compared to the entire study area. This further indicates that the best MOS may not be appropriately selected. However, in our case, the extent of 17.6% was chosen as the best transect size (and location), because it generates a relatively low error using a small amount of lidar data, and it has low within-object variability, thus enhancing discrimination between different height classes (Fig. 4).

Table 3 defines two models for both canopy-types, i.e., conifer and deciduous. These models represent an example of using a 17.6% lidar extent and a MOS of 0.04 ha. The RMSE are 6.0 m and 6.8 m for conifers and deciduous trees respectively, for the entire study area. Compared to deciduous trees, the canopy heights of conifers were better estimated. This can be explained by their relatively uniform shapes that facilitate canopy height estimation. In terms of the variables used in our models, all spectral, image-texture (i.e., both internal-object texture and GEOTEX) and shadow fraction variables proved beneficial to estimate forest canopy height for both models at this MOS. Spatial interpolation techniques (e.g., Kriging), were not

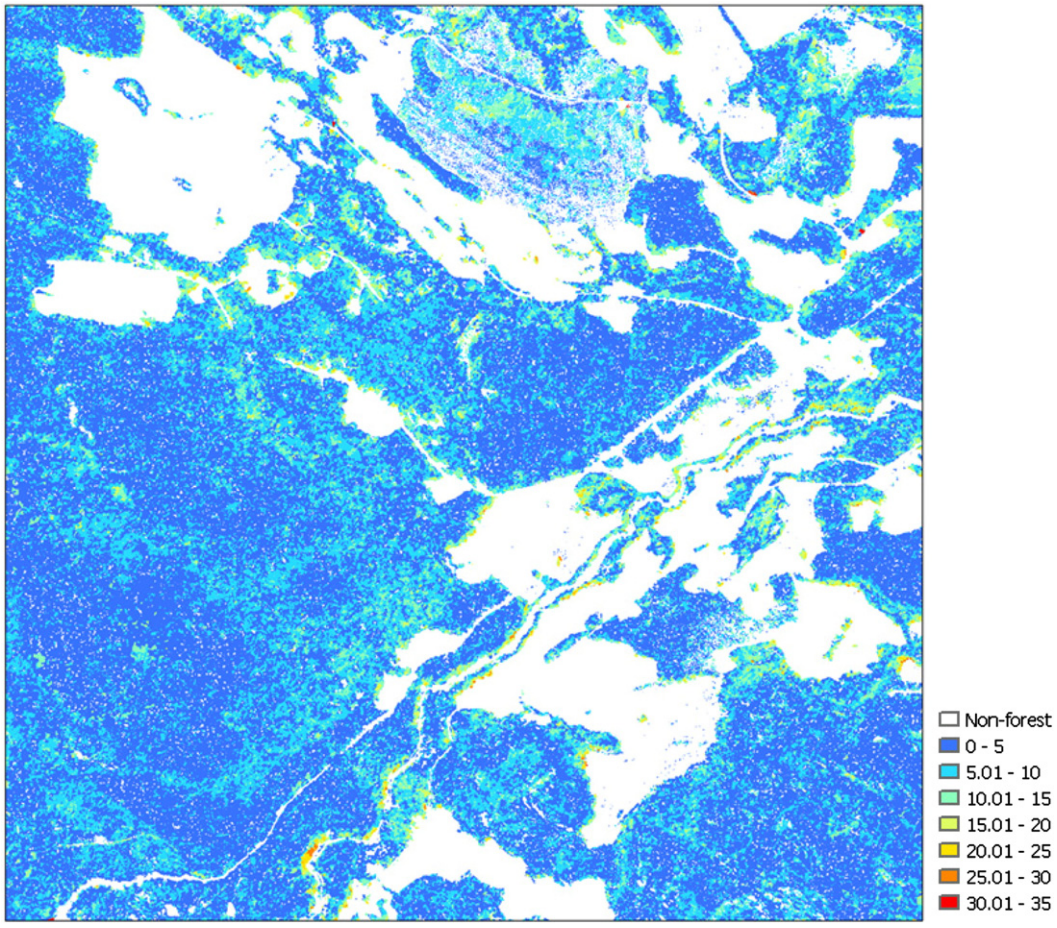

Fig. 10. Error image derived from a lidar transect extent of 17.6% and a MOS of 0.04 ha showing an error class interval of 5 m for the entire study area.

Table 4
Confusion matrix for analyzing the prediction errors of five height classes.

Estimated height (pixels)	Reference lidar height (pixels)					Row total	User's accuracy	Errors of commission
	HTC1[a]	HTC2[b]	HTC3[c]	HTC4[d]	HTC5[e]			
HTC1	2381	0	0	0	0	2381	2381/2381	0/2381
HTC2	893	2183	0	0	0	3076	2183/3076	893/3076
HTC3	235	2775	8904	143	0	12,057	8904/12,057	3153/12,057
HTC4	1	24	926	1256	0	2207	1256/2207	951/2207
HTC5	1	3	78	456	0	538	0/538	538/538
Column total	3511	4985	9908	1855	0	20,259		
Producer's accuracy	2381/3511	2183/4985	8904/9908	1256/1855	0/0		Overall accuracy = 72.68%	
Errors of omission	1130/3511	2802/4985	1004/9908	599/1855	0/0		Kappa coefficient = 0.58	

[a] HTC1: height class 1 (2–10.4 m).
[b] HTC2: height class 2 (10.5–19.4 m).
[c] HTC3: height class 3 (19.5–28.4 m).
[d] HTC4: height class 4 (28.5–37.4 m).
[e] HTC5: height class 5 (37.5–46.4 m).

used in this research, as these techniques have shown the potential to produce lower canopy height estimation accuracies than those applying multiple regression while using 'small' lidar transect extents (Hudak et al., 2002).

Fig. 10 illustrates a spatial distribution of height error derived from a lidar extent of 17.6% and a MOS of 0.04 ha. An error class interval of 5.0 m was used to show error detail. By comparing this figure with the lidar and QB images (Fig. 1), we can see that large homogeneous areas tend to exhibit lower error (<5.0 m). This suggests that these models are suitable for areas of relatively homogenous forest structure. However, errors (>5.0 m) were found among the mixed areas, containing both deciduous and conifer canopies, and the edge areas (beside clearcuts and river), where elevation, slope and aspect change abruptly and where trees typically exhibit variable growth. However, in total, approximately 91% of the forest canopies within this site contain errors less than one British Columbia (BC) forest inventory height class interval (i.e., ≈9.0 m). A confusion matrix (Table 4) was also constructed to analyze the prediction errors of five height classes (Table 1). A stratified random sampling method was used to extract validation points (0.1% of each height class) from the forested area in lidar CHS, with a total sample size of 20,259. Table 4 shows an overall accuracy of 72.68% with a kappa coefficient of 0.58. We notice that the height class 5 was entirely misclassified. There are two potential reasons: first, this class accounted for a very small portion of the study area (i.e., 0.07%) and our model was biased to the canopies with large portions. Second, the discretization of the continuous variable (i.e., canopy height) into five classes may introduce extra errors in confusion matrix. If a height value is on the boundary of two adjacent classes, the predicted height and the lidar height may be classified into different classes. For example, a lidar height of 18.0 m belongs to the height class 2; however, the corresponding predicted height of 20.0 m will be classified into the height class 3, although they only have 2.0 m difference.

As previously noted, several studies, such as Wulder and Seemann (2003) and Hilker et al. (2008), have combined lidar transects and optical data to estimate canopy height at the object level. However, their results were evaluated using only one type of MOS, which were much larger object sizes than defined in this research. The MOS in Wulder and Seemann (2003) was larger than 14 ha. Although no MOS information was reported in Hilker et al. (2008), it is estimated that most objects were larger than 2 ha, as this size typically represents the minimum BC forest inventory unit. Compared to these studies, our estimates were evaluated at multiscales (i.e., different mean object sizes) with the best canopy height estimation result derived at the much smaller canopy level (i.e., tree/cluster of 0.04 ha). Though our overall error is larger [i.e., 6.2 m versus 3.2 m in Wulder and Seemann (2003) and 3.5 m in Hilker et al. (2008)], we suggest that canopy height variability is better retained with smaller object sizes, which is important for fine-scale forest management (e.g., precision forestry). Additionally, the lidar transect locations in previous studies were heuristically defined without considering the canopy height spatial distribution.

5. Conclusion

In this study, we have developed a novel airborne lidar sampling strategy to determine three important lidar transect features (i.e., location, direction and extent). We further applied multiple regression models to investigate the amount of canopy height variability explained out of the full-scene variance by using high-resolution Quickbird imagery and (sampled) lidar transects within a GEOBIA (*Geographic Object-Based Image Analysis*) framework. Based on the results of this study, the following conclusions can be made:

- A pseudo-height map was generated using only QB imagery as the basis to determine appropriate locations to acquire lidar transects. Compared to the canopy height variability directly measured from lidar, the optical pseudo-height variability contains larger errors. However, it is important to have a good understanding of how and where canopy height is distributed in a study area before acquiring expensive lidar transects. As demonstrated in this study, QB data provide an effective way to generate a full-scene pseudo-height map based on high-resolution optical characteristics (e.g., texture and shadow).
- The lidar transect selection algorithm was based on the pseudo-height map, and three main rules. However, they are not fixed rules, but instead, can be tailored to meet different landscape conditions and project requirements, e.g., biased to small-cover or large-height classes for selective logging, or specific forest-types, (i.e., only deciduous). In our case, these rules were defined to assess all height classes for both forest types as per our research goals.
- The canopy height estimation models for this site have similar performance in north–south and west–east directions. Thus, lidar acquisition could take place in either direction.
- By using a *mean object size* (MOS) of 0.04 ha, a minimum lidar extent of 17.6% was found to achieve a similar result as those modeled from the full lidar scene. Specifically, the corresponding conifer and deciduous canopy height estimate errors were 6.0 m and 6.8 m, with a combined area-weighted error of 6.2 m. Furthermore, approximately 91% of all canopy heights in this site contain errors less than one British Columbia forest inventory height class interval (i.e., ≈9 m). It should be noted that, compared to the standard deviation (i.e., 8.0 m) of lidar-measured forest height, our estimation error still remains large. This requires further considerations using more robust generalization approaches, such as machine learning, instead of multiple regression.
- GEOBIA requires critical considerations regarding the selection of an appropriate (i.e., optimal) MOS. This research shows that the

best MOS (i.e., that leading to the lowest RMSE) derived from a lidar transect-covered area, may not guarantee the best result for the entire study area.

- This study shows that different lidar transect data (based on size and sample location) generate very different estimates (as well as errors) of canopy height. Thus, judicious decisions regarding the selection of lidar transect features are critical to develop robust integrated models. In addition to canopy height estimation accuracy, the selection of the 'best' lidar transects may also rely on other factors, such as site accessibility and budget.

6. Future work

This pilot study provides an initial framework for determining appropriate lidar transect features from optical imagery over a relatively small study area (i.e., 2600 ha). Ironically, it was the high initial acquisition costs for this relatively small area, which prompted this study. However, operational potential requires this framework to be calibrated and validated using geographically larger datasets. This is currently underway on two different sites, based on lessons learned here.

Acknowledgments

This research has been funded by an Alberta Ingenuity Fund (AIF) and an Alberta Informatics Circle of Research Excellence (iCore) PhD scholarship awarded to Gang Chen. Dr. Hay acknowledges support from a Natural Sciences and Engineering Research Council (NSERC) Discovery Grant and an AIF New Faculty Award. We appreciate the generous use of Quickbird and lidar data provided by Dr. Benoît St-Onge at the University of Quebec at Montreal, and the valuable discussions with John Andres at the British Columbia Ministry of Forests and Range.

References

Castilla, G., Hay, G. J., & Ruiz, J. R. (2008). Size-constrained region merging (SCRM): An automated delineation tool for assisted photointerpretation. *Photogrammetric Engineering and Remote Sensing*, *74*, 409−419.

Chen, G., Hay, G. J., Castilla, G., St-Onge, B., & Powers, R. (2010). A multiscale geographic object-based image analysis (GEOBIA) to estimate lidar-measured forest canopy height using Quickbird imagery. *International Journal of Geographical Information Science*. doi:10.1080/13658816.2010.496729

Donoghue, D. N. M., & Watt, P. J. (2006). Using LiDAR to compare forest height estimates from IKONOS and Landsat ETM+ data in Sitka spruce plantation forests. *International Journal of Remote Sensing*, *27*, 2161−2175.

Dougherty, E. R., & Lotufo, R. A. (2003). *Hands-on morphological image processing* (pp. 163−192). Bellingham: SPIE Optical Engineering Press.

Franklin, S. E., & McDermid, G. J. (1993). Empirical relations between digital SPOT HRV and CASI spectral response and lodgepole pine (*Pinus contorta*) forest stand parameters. *International Journal of Remote Sensing*, *14*, 2331−2348.

Hay, G. J., & Blaschke, T. (2010). Special issue on Geographic Object-Based Image Analysis (GEOBIA): Foreword. *Photogrammetric Engineering and Remote Sensing*, *76*, 121−122.

Hay, G. J., & Castilla, G. (2008). Geographic Object-Based Image Analysis (GEOBIA). In T. Blaschke, S. Lang, & G. J. Hay (Eds.), *Object-Based Image Analysis — Spatial concepts for knowledge-driven remote sensing applications* (pp. 77−92). Berlin: Springer-Verlag.

Hay, G. J., Castilla, G., Wulder, M. A., & Ruiz, J. R. (2005). An automated object-based approach for the multiscale image segmentation of forest scenes. *International Journal of Applied Earth Observation and Geoinformation*, *7*, 339−359.

Hay, G. J., Marceau, D. J., Dube, P., & Bouchard, A. (2001). A multiscale framework for landscape analysis: Object-specific analysis and upscaling. *Landscape Ecology*, *16*, 471−490.

Hay, G. J., Niemann, K. O., & McLean, G. F. (1996). An object-specific image-texture analysis of H-resolution forest imagery. *Remote Sensing of Environment*, *55*, 108−122.

Hay, G. J. (1993). Visualizing 3-D texture: A three dimensional structural approach to model forest texture. Unpublished MSc Thesis, University of Victoria.

Hilker, T., Wulder, M. A., & Coops, N. C. (2008). Update of forest inventory data with lidar and high spatial resolution satellite imagery. *Canadian Journal of Remote Sensing*, *34*, 5−12.

Horn, B. K. P., & Brooks, M. J. (1989). *Shape from shading*. Cambridge, MA: The MIT Press.

Hudak, A. T., Lefsky, M. A., Cohen, W. B., & Berterreche, M. (2002). Integration of LIDAR and Landsat ETM+ data for estimating and mapping forest canopy height. *Remote Sensing of Environment*, *82*, 397−416.

Hyde, P., Dubayah, P., Walker, W., Blair, J. B., Hofton, M., & Hunsaker, C. (2006). Mapping forest structure for wildlife habitat analysis using multi-sensor (LiDAR, SAR/InSAR, ETM+, Quickbird) synergy. *Remote Sensing of Environment*, *102*, 26−36.

Hyyppä, J., Hyyppä, H., Leckie, D., Gougeon, F., Yu, X., & Maltamo, M. (2008). Review of methods of small-footprint airborne laser scanning for extracting forest inventory data in boreal forests. *International Journal of Remote Sensing*, *29*, 1339−1366.

Jarvis, R. A. (1983). A perspective on range finding techniques for computer vision. *IEEE Transactions on Pattern Analysis and Machine Intelligence*, *PAMI-5*, 122−139.

Lefsky, M. A., Cohen, W. B., Harding, D. J., Parkers, G. G., Acker, S. A., & Gower, S. T. (2002). Lidar remote sensing of above-ground biomass in three biomes. *Global Ecology & Biogeography*, *11*, 393−399.

Lillesand, T. M., Kiefer, R. W., & Chipman, J. W. (2007). *Remote sensing and image interpretation* (pp. 240−249). (6th Edition). New Jersey: John Wiley & Sons, Inc.

Lim, K., Treitz, P., Baldwin, K., Morrison, I., & Green, J. (2003). Lidar remote sensing of biophysical properties of tolerant northern hardwood forests. *Canadian Journal of Remote Sensing*, *29*, 658−678.

Means, J. E., Acker, S. A., Harding, D. J., Blair, J. B., Lefsky, M. A., Cohen, W. B., et al. (1999). Use of large-footprint scanning airborne lidar to estimate forest stand characteristics in the Western Cascades of Oregon. *Remote Sensing of Environment*, *67*, 298−308.

MFR (Ministry of Forests and Range), the British Columbia Government, Canada (2010). https://psc2.for.gov.bc.ca/RESULTS/HELP/Results_Online_Help/Pop_ups/pop_Height_Class.htm

Morgenstern, K., Black, T. A., Humphreys, E. R., Griffis, T. J., Drewitt, G. B., Cai, T. B., et al. (2004). Sensitivity and uncertainty of the carbon balance of a Pacific Northwest Douglas-fir forest during an El Nino La Nina cycle. *Agricultural and Forest Meteorology*, *123*, 201−219.

O'Neill, R. V., Hunsaker, C. T., Timmins, S. P., Jackson, B. L., Jones, K. B., Ritters, K. H., et al. (1996). Scale problems in reporting landscape patterns at the regional scale. *Landscape Ecology*, *11*, 169−180.

Strahler, A., Woodcock, C., & Smith, J. (1986). On the nature of models in remote sensing. *Remote Sensing of Environment*, *20*, 121−139.

Tou, J. T., & Gonzalez, R. C. (1974). *Pattern recognition principles* (pp. 97−104). Reading, MA: Addison-Wesley Publishing Company.

Welch, R., & Ahlers, W. (1987). Merging multiresolution SPOT HRV and Landsat TM data. *Photogrammetric Engineering and Remote Sensing*, *53*, 301−303.

Wulder, M. A., & Seemann, D. (2003). Forest inventory height update through the integration of LIDAR data with segmented Landsat imagery. *Canadian Journal of Remote Sensing*, *29*, 536−543.